Topological Quantum Optics in Two-Dimensional Atomic Arrays

J. Perczel,[1,2] J. Borregaard,[2] D. E. Chang,[3] H. Pichler,[2,4] S. F. Yelin,[2,5] P. Zoller,[6,7] and M. D. Lukin[2]
[1]Physics Department, Massachusetts Institute of Technology, Cambridge, Massachusetts 02139, USA
[2]Physics Department, Harvard University, Cambridge, Massachusetts 02138, USA
[3]ICFO—Institut de Ciencies Fotoniques, The Barcelona Institute of Science and Technology, 08860 Castelldefels, Barcelona, Spain
[4]ITAMP, Harvard-Smithsonian Center for Astrophysics, Cambridge, Massachusetts 02138, USA
[5]Department of Physics, University of Connecticut, Storrs, Connecticut 06269, USA
[6]Institute for Theoretical Physics, University of Innsbruck, A-6020 Innsbruck, Austria
[7]Institute for Quantum Optics and Quantum Information of the Austrian Academy of Sciences, A-6020 Innsbruck, Austria
(Received 14 March 2017; published 14 July 2017)

We demonstrate that two-dimensional atomic emitter arrays with subwavelength spacing constitute topologically protected quantum optical systems where the photon propagation is robust against large imperfections while losses associated with free space emission are strongly suppressed. Breaking time-reversal symmetry with a magnetic field results in gapped photonic bands with nontrivial Chern numbers and topologically protected, long-lived edge states. Due to the inherent nonlinearity of constituent emitters, such systems provide a platform for exploring quantum optical analogs of interacting topological systems.

DOI: 10.1103/PhysRevLett.119.023603

Charged particles in two-dimensional systems exhibit exotic macroscopic behavior in the presence of magnetic fields and interactions. These include the integer [1], fractional [2], and spin [3] quantum Hall effects. Such systems support topologically protected edge states [4,5] that are robust against defects and disorder. There is a significant interest in realizing topologically protected photonic systems. Photonic analogs of quantum Hall behavior have been studied in gyromagnetic photonic crystals [6–11], helical waveguides [12], two-dimensional lattices of optical resonators [13–15] and in polaritons coupled to optical cavities [16]. An outstanding challenge is to realize optical systems which are robust not only to some specific backscattering processes but to *all* loss processes, including scattering into unconfined modes and spontaneous emission. Another challenge is to extend these effects into a nonlinear quantum domain with strong interactions between individual excitations. These considerations motivate the search for new approaches to topological photonics.

In this Letter, we introduce and analyze a novel platform for engineering topological states in the optical domain. It is based on atomic or atomlike quantum optical systems [17], where time-reversal symmetry can be broken by applying magnetic fields and the constituent emitters are inherently nonlinear. Specifically, we focus on optical excitations in a two-dimensional honeycomb array of closely spaced emitters. We show that such systems maintain topologically protected confined optical modes that are immune to large imperfections as well as to the most common loss processes such as scattering into free-space modes. Such modes can be used to control individual atom emission, and to create quantum nonlinearity at a single photon level.

The key idea is illustrated in Fig. 1(a). We envision an array with interatomic spacing a and quantization axis $\hat{z}$

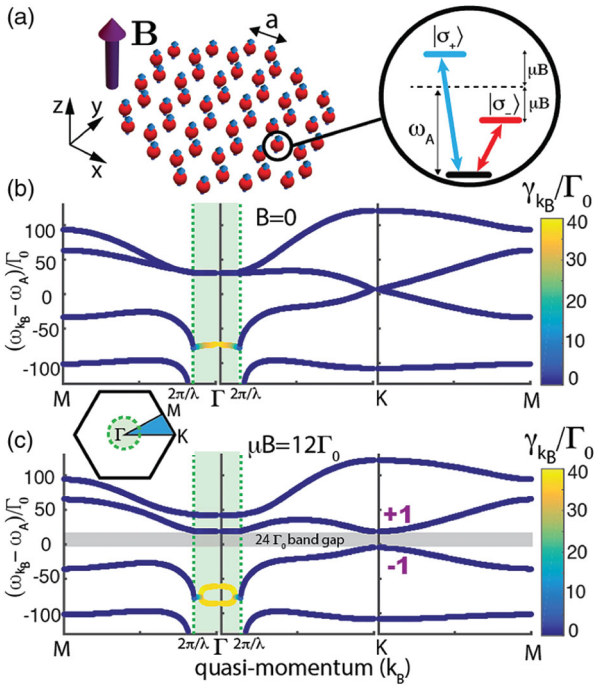

FIG. 1. (a) Honeycomb lattice of atomic emitters with interatomic spacing a. Each atom has a V-type level structure with optical transitions to the $|\sigma_+\rangle$ and $|\sigma_-\rangle$ states. A magnetic field breaks the degeneracy via the Zeeman splitting. (b) Band structure of the lattice with $B = 0$. Green dashed lines indicate the edges of the free-space light cone. Modes with quasimomentum $k_B < \omega_{\mathbf{k}_B}/c$ couple to free-space modes and are short lived (green shaded region). Decay rates of the modes are color coded. Bands are degenerate at the symmetry points $\mathbf{K}$ and $\mathbf{\Gamma}$. (c) A transverse magnetic field ($\mu B = 12\Gamma_0$) opens a gap (grey shaded region) between topological bands with nontrivial Chern numbers. Relevant parameters are $\lambda = 790\,\mathrm{nm}$, $\Gamma_0 = 2\pi \times 6\,\mathrm{MHz}$, and $a = 0.05\lambda$.

perpendicular to the plane of the atoms. Each emitter has a V-type level structure with transitions from the ground state to the excited states $|\sigma_+\rangle$ and $|\sigma_-\rangle$, excited by the corresponding polarization of light [18]. The hybridized atomic and photonic states result in confined Bloch modes with large characteristic quasimomenta that for dense atomic arrays significantly exceed the momentum of free-space photons. These confined modes are outside of the so-called "light cone" and are decoupled from free space resulting in long-lived, subradiant states [19]. Atomic Zeeman shifts induced by a magnetic field create a band gap in the optical excitation spectrum, and the Bloch bands acquire nontrivial Chern numbers. The resulting system displays all essential features associated with topological robustness. Before proceeding, we note that polar molecules coupled via near-field interactions [21,22] and excitons in Moiré heterojunctions [23] have been shown to give rise to chiral excitations in 2D. In contrast, the present analysis includes both near- and far-field effects as well as scattering to free space. We also note that the emergence of Weyl excitations has been recently predicted [24] in 3D lattices of polar particles.

In the single excitation case, following the adiabatic elimination of the photonic modes, the dynamics of the system (no-jump evolution in the master equation [25]) can be described by the following non-Hermitian spin Hamiltonian [17,26–29]

$$H = \hbar \sum_{i=1}^{N} \sum_{\alpha=\sigma_+,\sigma_-} \left(\omega_A + \mathrm{sgn}(\alpha_i)\mu B - \mathrm{i}\frac{\Gamma_0}{2}\right)|\alpha_i\rangle\langle\alpha_i| + \frac{3\pi\hbar\Gamma_0 c}{\omega_A} \sum_{i\neq j} \sum_{\alpha,\beta=\sigma_+,\sigma_-} G_{\alpha\beta}(\mathbf{r}_i - \mathbf{r}_j)|\alpha_i\rangle\langle\beta_j|, \quad (1)$$

where N is the number of atoms, $\omega_A = 2\pi c/\lambda$ is the atomic transition frequency with wavelength λ, μB is the Zeeman-shift of the atoms with magnetic moment μ due to an out-of-plane magnetic field $\mathbf{B} = B\hat{z}$ with $\mathrm{sgn}(\sigma_\pm) = \pm$. Here, $\Gamma_0 = d^2\omega_A^3/(3\pi\epsilon_0\hbar c^3)$ is the radiative linewidth of an individual atom in free space, c is the speed of light, d is the transition dipole moment, $G_{\alpha\beta}(\mathbf{r})$ is the dyadic Green's function in free space describing the dipolar spin-spin interaction [30], and $\mathbf{r}_i$ denotes the position of the atoms. Note that the Hamiltonian in Eq. (1) assumes the atoms are pinned to the lattice. The effect of fluctuating atomic positions is discussed in Ref. [30].

For an infinite periodic honeycomb lattice, the single excitation eigenmodes of Eq. (1) are Bloch modes [38] given by

$$|\psi_{\mathbf{k}_B}\rangle = \sum_n \sum_{b=1,2} e^{\mathrm{i}\mathbf{k}_B\cdot\mathbf{R}_n}[c^b_{+,\mathbf{k}_B}|\sigma^b_{+,n}\rangle + c^b_{-,\mathbf{k}_B}|\sigma^b_{-,n}\rangle], \quad (2)$$

where the summation runs over all lattice vectors $\{\mathbf{R}_n\}$, $b = 1, 2$ labels the two atoms within the unit cell, and $\mathbf{k}_B$ is the Bloch wave vector. For each $\mathbf{k}_B$ there are four eigenvalues of the form $E_{\mathbf{k}_B} = \omega_{\mathbf{k}_B} - \mathrm{i}\gamma_{\mathbf{k}_B}$, where the imaginary part corresponds to the overall decay rate of the modes [30].

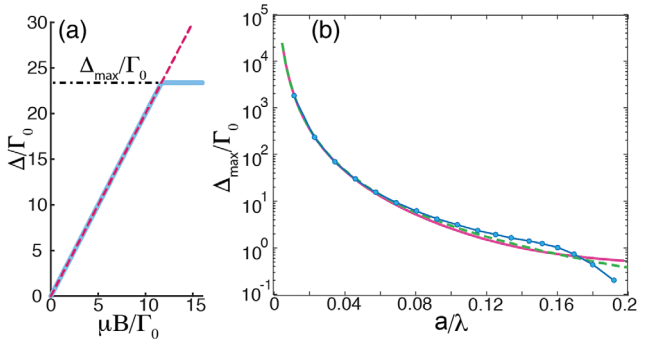

FIG. 2. (a) Size of the gap between topological bands (blue line) as a function of magnetic field for $a = \lambda/20$. (b) The maximum gap size $\Delta_{\max}$ (blue dotted line) as a function of the interatomic spacing a. The solid magenta line shows the dipolar interaction strength J between two atoms with parallel dipole moments. The dashed green line is a phenomenological $J \sim 1/r^3$ fit. For $a \ll \lambda$, $\Delta_{\max}$ scales as $1/a^3$.

Figure 1(b) shows the band structure in the absence of a magnetic field along the lines joining the symmetry points $\mathbf{M}$, $\mathbf{\Gamma}$, and $\mathbf{K}$ of the irreducible Brillouin zone [see inset of Fig. 1(c)]. The decay rates of the modes ($\gamma_{\mathbf{k}_B}$) are shown using a color code. Crucially, we find that the decay rate of some modes can be significantly smaller than $\Gamma_0/2$ due to collective interference effects. Green dashed lines at $k_B = 2\pi/\lambda$ mark the edges of the light cone corresponding to free space modes with dispersion $\omega_{\mathbf{k}_B} = k_B c$. The modes close to the center of the Brillouin zone ($\mathbf{\Gamma}$) have quasimomenta k_B less than the maximum momentum of free space photons at the same energy ($k_\mathrm{B} < \omega_{\mathbf{k}_B}/c$). These modes couple strongly to free-space modes with matching energy and momentum and decay rapidly [30]. In contrast, modes with quasimomenta greater than the momentum of free space photons ($k_\mathrm{B} > \omega_{\mathbf{k}_B}/c$) are completely decoupled and do not decay into free space due to the momentum mismatch.

Figure 1(b) also shows that the photonic bands are degenerate at the symmetry points $\mathbf{\Gamma}$ and $\mathbf{K}$ in the absence of a magnetic field. These degeneracies originate from the degeneracy of the $|\sigma_+\rangle$ and $|\sigma_-\rangle$ states at zero magnetic field. Due to the lattice symmetries, the degeneracy at the $\mathbf{\Gamma}$ point is quadratic [39], while a linear Dirac cone is formed at the $\mathbf{K}$ point [7]. Applying an out-of-plane magnetic field lifts this degeneracy and an energy gap forms across the Brillouin zone.

We explore the topological nature of these bands, by calculating the Chern numbers using the method described in Ref. [40]. The sum of the Chern numbers above and below the band gap is $+1$ and -1, respectively. The origin of these topological bands can be understood intuitively by noting that at the $\mathbf{K}$ point the modes separated in energy

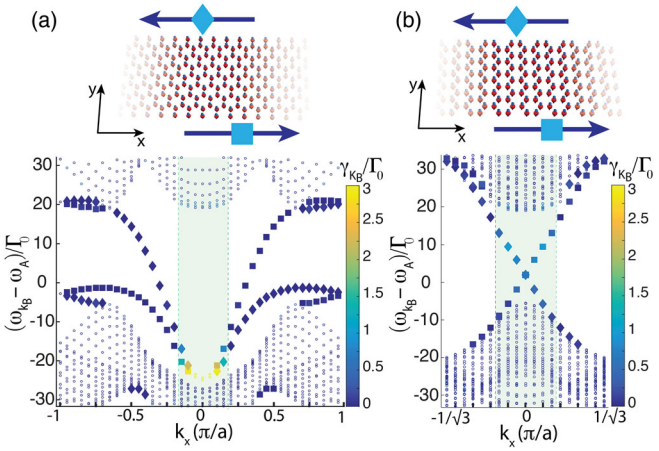

FIG. 3. Topological edge states on the (a) bearded and (b) armchair edges of periodic stripes of atoms. Each edge supports only one unidirectional mode. Modes propagating on the upper (lower) edges of the stripes are marked by diamonds (squares) in the band diagrams. Bulk modes are marked with dots. Decay rates of the modes are color coded. Modes of the bearded (armchair) edges cross the gap with quasimomentum $k_B > \omega_{\mathbf{k}_B}/c$ ($k_B < \omega_{\mathbf{k}_B}/c$) making them long (short) lived. Parameters are the same as in Fig. 1(c). The spectrum was obtained for the bearded (armchair) edges from a 40×42 (40×41) lattice of atoms with periodic boundary conditions along the first dimension. States for which the ratio of the total amplitude on the top (bottom) four atom rows to the bottom (top) four rows is greater than 15 are classified as edge states.

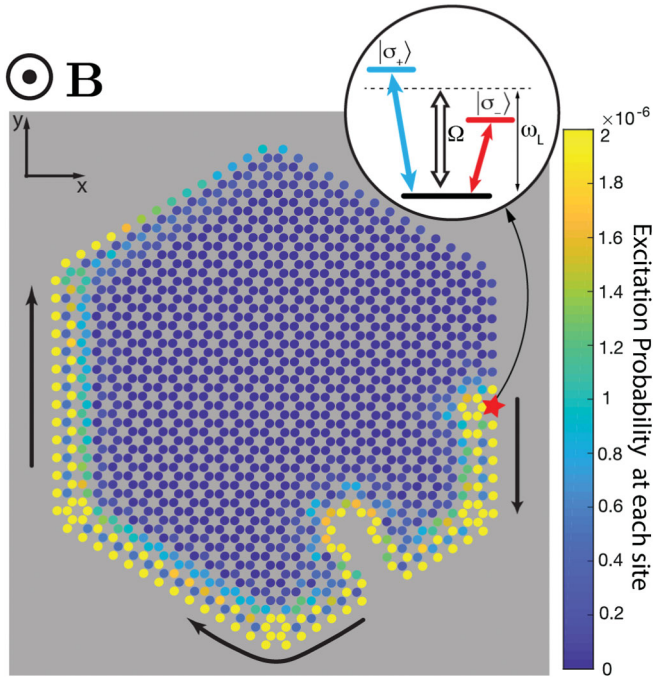

FIG. 4. Snapshot of the time evolution (at $t = 5.7\Gamma_0^{-1}$) of the system as an atom on the edge (red star) is driven by a laser (inset). The color code shows the excitation probability $|\langle\psi(t)|\sigma_+^i\rangle|^2 + |\langle\psi(t)|\sigma_-^i\rangle|^2$ at each atomic site $i = 1, \ldots, N$. Approximately 96% of the emitted excitation is coupled into the forward direction and scattering into bulk and backward edge modes is strongly suppressed. The excitation goes around corners and routes around the large lattice defect. Relevant parameters are $N = 1243$, $\lambda = 790$ nm, $\Gamma_0 = 2\pi \times 6$ MHz, $a = 0.05\lambda$, and $\mu B = 12\Gamma_0$. The strength of the drive is $\Omega = 1/5\Gamma_0$ and the driving frequency is $\omega_L = \omega_A + 15\Gamma_0$. The driving laser is adiabatically switched on with a Gaussian profile $\Omega(t) = \Omega \exp(-[t - 1.5\Gamma_0^{-1}]^2/[0.15\Gamma_0^{-2}])$ for $t < 1.5\Gamma_0^{-1}$.

due to Zeeman splitting have, respectively, $\hat{\sigma}_+$ and $\hat{\sigma}_-$ circular polarizations. The opposite chirality of the bands reflects the time-dependent circular rotation of the electric fields associated with the $\hat{\sigma}_+$ and $\hat{\sigma}_-$ polarizations in the x-y plane.

The size of the topological gap at the $\mathbf{K}$ point scales linearly with the magnetic field due to the Zeeman splitting ($2\mu B$) of the $|\sigma_+\rangle$ and $|\sigma_-\rangle$ states [Fig. 2(a)], but the gap size is eventually limited to a maximum value $\Delta_{\max}$ due to the level repulsion between the two upper bands at the $\mathbf{\Gamma}$ point. Figure 2(b) shows the maximum gap size as a function of the interatomic spacing a (blue dotted line). The strength of the dipolar coupling $J = 3\pi\Gamma_0 c/\omega_A G_{xx}(a)$ between two parallel dipoles at a distance a is also shown. The close agreement between the two curves shows that the maximum gap size is determined by the dipolar interaction strength between the atoms. For $a \ll \lambda$ the maximum gap size has the simple scaling $\Delta_{\max} \sim 1/a^3$.

Gaps between topological bands are typically associated with the presence of one-way reflection-free edge modes at the boundaries of a finite system. To explore the spectrum of edge modes in the gap, we calculated the band structure for periodic stripes of atoms in a honeycomb lattice. The stripes may have bearded, armchair, or zig-zag edges [41,42]. Figure 3 shows the edge geometries and the corresponding band structures of stripes with bearded and armchair edges. Zig-zag edges are discussed in Ref. [30]. Edge modes on the lower (upper) edge of the stripe traversing the gap have positive (negative) group velocity and carry energy to the right (left). Thus, energy transport by edge modes is unidirectional as a consequence of the broken time-reversal symmetry of the system. If the direction of the magnetic field is flipped, the direction of the energy flow on any given edge is reversed. Edge modes on bearded boundaries have quasimomenta $k_B > \omega_{\mathbf{k}_B}/c$ while crossing the gap and therefore couple weakly to free-space modes making them long lived. In contrast, modes on the armchair edges cross the gap with quasimomenta $k_B < \omega_{\mathbf{k}_B}/c$ and the relatively strong coupling to free-space modes makes them short lived. The lifetimes of edge modes are also influenced by the lattice size. Increasing the number of atoms N in a finite lattice decreases the losses from finite-size effects and increases the lifetimes of long-lived edge modes [30].

Figure 4 illustrates the unidirectional energy transport. It shows a honeycomb lattice of atoms with an overall hexagonal shape and a large defect on one edge. The

geometry was chosen such that in the absence of defects, all boundaries are bearded edges supporting long-lived edge modes. An out-of-plane magnetic field $\mathbf{B}$ induces a band gap of size Δ in the energy spectrum. An atom on the boundary is adiabatically addressed by a laser at a frequency ω_L resonant with the long-lived edge modes in the topmost part of the band gap. The laser drives the σ_+ and σ_- transitions of the atom off-resonantly with equal coupling strengths Ω, where $\Omega \ll \Delta$. Figure 4 shows a snapshot of the excitation probability of each atom in the lattice. Approximately 96% of the excitation emitted by the driven atom is coupled into the edge modes carrying energy in the forward direction. Coupling into the backward direction or into the bulk modes is suppressed due to topology and the large band gap. These results are qualitatively independent of the relative driving strengths of the σ_- and σ_+ transitions [30]. The excitation routes around lattice corners with ~97% efficiency and goes around defects of arbitrary shape and size by forming new edge modes at the defect boundaries as shown in Fig. 4, where ~83% of the excitation survives. Atomic emission in the bulk is discussed in Ref. [30].

The distance the photon propagates on an edge is set by the ratio of the group velocity and the intrinsic lifetime of the edge modes. The group velocity of the edge modes traversing the gap is $v_g \approx \delta\omega/\delta k_B \sim \Delta/(\pi/a)$, where Δ is the size of the energy gap and a is the interatomic spacing. Thus for $a \ll \lambda$, the maximum group velocity of the edge modes scales as $v_g \sim \Delta_{max}/(\pi/a) \sim a^{-2}$. While bearded edges support long-lived modes, any departure from the ideal hexagonal shape of Fig. 4 creates a combination of armchair and zig-zag modes that couple more strongly to free-space modes and thus have limited lifetimes. To ensure that only a small fraction of the excitation is lost while the photon is routed around a defect, large group velocities and, therefore, small interatomic spacing is required.

We note that efficient coupling of individual quantum emitters to a confined unidirectional channel (Fig. 4) immediately implies the feasibility of quantum nonlinear interactions between individual photons. This can be understood by considering a "defect atom" placed along the path of the edge excitation. Such an atom can be used to capture and store an incident photon in a long-lived atomic state, following e.g. Ref. [43] (see also Refs. [44–47]). After photon storage, the defect atom will form a lattice defect for subsequent incoming photons, which will be routed around this defect and, as a result, will acquire a nonlinear phase shift.

Atomic arrays with much smaller interatomic spacing than the transition wavelength ($a \ll \lambda$) could be experimentally realized using state-of-the-art experiments with bosonic Stronium atoms [24,48]. Mott insulators in the $^1S_0$ ground state of ^{84}Sr atoms using a 532 nm trapping laser have been realized experimentally [49] and the atoms can be further transferred to the metastable $^3P_0$ state [50]. Using the long-wavelength $^3P_0$–$^3D_1$ transition with $\lambda_{Sr} = 2.6$ μm for atom-atom interactions would give $a = 2\lambda_{laser}/(3\sqrt{3}) = \lambda_{Sr}/12.7$ in an optical honeycomb lattice. The interatomic spacing could be further reduced to $a = \lambda_{Sr}/16.3$ using a 412.8 nm "magic wavelength" trapping laser providing equal confinement for the $^3P_0$ and $^3D_1$ states [48]. Typical trapping frequencies in Mott insulators are $\sim 5E_{recoil}/h$ [51], where $E_{recoil}/h \approx 13$ kHz for Stronium. Since the linewidth is $\Gamma_{Sr} = 290$ kHz for the $^3P_0$–$^3D_1$ transition, the motional states of individual atoms are not well resolved and we expect heating due to photon scattering to be small. The main experimental challenge is to ensure near-unity lattice filling [52] and near-uniform excitation of atoms to the $^3P_0$ state. Other approaches to deep subwavelength atomic lattices include utilizing vacuum forces in the proximity of dielectrics [53], using adiabatic potentials [54], dynamic modulation of optical lattices [55], or subwavelength positioning of atomlike color defects in diamond nanophotonic devices [56–59] [60].

Subwavelength emitter lattices could also be created using monolayer semiconductors, such as transition metal dichalcogenides (TMDCs) [61–66]. Large splitting of the σ_+, σ_- valley polarizations due to interaction-induced paramagnetic responses was recently demonstrated in TMDCs [67]. Moiré patterns [68] could provide deep subwavelength ($a < 36$ nm) periodic potentials for TMDC excitons and give rise to topological bands and chiral excitonic edge states [23]. In such Moiré heterojunctions the band gaps—and thus the group velocities of edge states—are predicted to be small ($\Delta < 1\Gamma_0$). However, as our current analysis shows, edge states outside the light cone would be long lived and thus could still propagate a significant distance along the edges of TMDCs prior to decay into far field modes.

In summary, we have shown that two-dimensional atomic lattices can be used to create robust quantum optical systems featuring band gaps between photonic bands with nontrivial Chern numbers. For a finite lattice, unidirectional reflection-free edges states form on the system boundaries at energies inside the band gap. These edge modes are robust against imperfections in the lattice as well as scattering and emission into free space. These can be used, e.g., to control emission of individual atoms. We emphasize that, in contrast to linear topological photonic systems, a distinguishing feature of the present approach is the intrinsic, built-in nonlinearity associated with quantum emitters in the lattice, which leads to strong interactions between individual excitations. Harnessing such interactions could open up exciting possibilities for studying topological phenomena with strongly interacting photons, including quantum optical analogs of fractional quantum Hall states. These include exotic states, such as those with filling fractions $\nu = 5/2$ and $\nu = 12/5$, which may feature non-Abelian excitations [69]. In addition, the inherent protection against losses may also be used for the realization of robust quantum nonlinear optical devices for potential applications in quantum information processing and quantum state transfer [70].

We thank D. Wild, E. Shahmoon, A. High, T. Andersen, N. Yao, J. Taylor, D. Greif, S. Choi, A. Keesling, R. Evans, A. Sipahigil, P. Kómar, and M. Kanász-Nagy for illuminating discussions. We acknowledge funding from the MIT-Harvard Center for Ultracold Atoms, NSF, AFOSR, and MURI. J. P. acknowledges support from the Hungary Initiative Foundation. J. B. acknowledges funding from the Carlsberg Foundation. D. E. C. acknowledges support from the MINECO "Severo Ochoa" Program (SEV-2015-0522), Fundacio Privada Cellex, CERCA Programme/Generalitat de Catalunya, and ERC Starting Grant FOQAL. Work at Innsbruck is supported by SFB FOQUS of the Austrian Science Fund, and ERC Synergy Grant UQUAM.

[1] K. V. Klitzing, G. Dorda, and M. Pepper, Phys. Rev. Lett. **45**, 494 (1980).
[2] D. C. Tsui, H. L. Stormer, and A. C. Gossard, Phys. Rev. Lett. **48**, 1559 (1982).
[3] M. Konig, S. Wiedmann, C. Brune, A. Roth, H. Buhmann, L. W. Molenkamp, X.-L. Qi, and S.-C. Zhang, Science **318**, 766 (2007).
[4] B. I. Halperin, Phys. Rev. B **25**, 2185 (1982).
[5] R. B. Laughlin, Phys. Rev. B **23**, 5632 (1981).
[6] F. D. M. Haldane and S. Raghu, Phys. Rev. Lett. **100**, 013904 (2008).
[7] S. Raghu and F. D. M. Haldane, Phys. Rev. A **78**, 033834 (2008).
[8] Z. Wang, Y. D. Chong, J. D. Joannopoulos, and M. Soljačić, Phys. Rev. Lett. **100**, 013905 (2008).
[9] K. Liu, L. Shen, and S. He, Opt. Lett. **37**, 4110 (2012).
[10] Z. Wang, Y. Chong, J. D. Joannopoulos, and M. Soljačić, Nature (London) **461**, 772 (2009).
[11] Z. Yu, G. Veronis, Z. Wang, and S. Fan, Phys. Rev. Lett. **100**, 023902 (2008).
[12] M. C. Rechtsman, J. M. Zeuner, Y. Plotnik, Y. Lumer, D. Podolsky, F. Dreisow, S. Nolte, M. Segev, and A. Szameit, Nature (London) **496**, 196 (2013).
[13] M. Hafezi, E. A. Demler, M. D. Lukin, and J. M. Taylor, Nat. Phys. **7**, 907 (2011).
[14] M. Hafezi, S. Mittal, J. Fan, A. Migdall, and J. M. Taylor, Nat. Photonics **7**, 1001 (2013).
[15] K. Fang, Z. Yu, and S. Fan, Nat. Photonics **6**, 782 (2012).
[16] T. Karzig, C.-E. Bardyn, N. H. Lindner, and G. Refael, Phys. Rev. X **5**, 031001 (2015).
[17] E. Shahmoon, D. S. Wild, M. D. Lukin, and S. F. Yelin, Phys. Rev. Lett. **118**, 113601 (2017).
[18] For simplicity we assume that the $|z\rangle$ state is far detuned from resonance, e.g. due to Stark shift. However, one can include the $|z\rangle$ state without detuning as long as there are no polarization-mixing perturbations in the system, as radiation from the $|\sigma_+\rangle$ and $|\sigma_-\rangle$ states is completely decoupled from the $|z\rangle$ transition.
[19] Subradiance in periodic atomic lattices was also discussed recently, in the absence of topology, in Ref. [20].
[20] A. Asenjo-Garcia, M. Moreno-Cardoner, A. Albrecht, H. J. Kimble, and D. E. Chang, arXiv:1703.03382.
[21] N. Y. Yao, C. R. Laumann, A. V. Gorshkov, S. D. Bennett, E. Demler, P. Zoller, and M. D. Lukin, Phys. Rev. Lett. **109**, 266804 (2012).
[22] D. Peter, N. Y. Yao, N. Lang, S. D. Huber, M. D. Lukin, and H. P. Büchler, Phys. Rev. A **91**, 053617 (2015).
[23] F. Wu, T. Lovorn, and A. H. MacDonald, Phys. Rev. Lett. **118**, 147401 (2017).
[24] S. V. Syzranov, M. L. Wall, B. Zhu, V. Gurarie, and A. M. Rey, Nat. Commun. **7**, 13543 (2016).
[25] C. W. Gardiner and P. Zoller, *Quantum Noise: A Handbook of Markovian and Non-Markovian Quantum Stochastic Methods with Applications to Quantum Optics* (Springer, New York, 2010).
[26] J. Perczel *et al.* (to be published).
[27] M. Antezza and Y. Castin, Phys. Rev. Lett. **103**, 123903 (2009).
[28] T. Bienaimé, N. Piovella, and R. Kaiser, Phys. Rev. Lett. **108**, 123602 (2012).
[29] W. Guerin, M. O. Araújo, and R. Kaiser, Phys. Rev. Lett. **116**, 083601 (2016).
[30] See Supplemental Material at http://link.aps.org/supplemental/10.1103/PhysRevLett.119.023603, which includes Refs. [31–37], for more details.
[31] M. Antezza and Y. Castin, Phys. Rev. A **80**, 013816 (2009).
[32] O. Morice, Y. Castin, and J. Dalibard, Phys. Rev. A **51**, 3896 (1995).
[33] W. C. Chew, *Wave and fields in inhomogeneous media* (IEEE, 1999), p. 632.
[34] J. S. Douglas, H. Habibian, C.-L. Hung, A. V. Gorshkov, H. J. Kimble, and D. E. Chang, Nat. Photonics **9**, 326 (2015).
[35] H. T. Dung, L. Knöll, and D.-G. Welsch, Phys. Rev. A **57**, 3931 (1998).
[36] S. John and J. Wang, Phys. Rev. Lett. **64**, 2418 (1990).
[37] R. Mitsch, C. Sayrin, B. Albrecht, P. Schneeweiss, and A. Rauschenbeutel, Nat. Commun. **5**, 5713 (2014).
[38] C. Bena and G. Montambaux, New J. Phys. **11**, 095003 (2009).
[39] Y. D. Chong, X.-G. Wen, and M. Soljačić, Phys. Rev. B **77**, 235125 (2008).
[40] T. Fukui, Y. Hatsugai, and H. Suzuki, J. Phys. Soc. Jpn. **74**, 1674 (2005).
[41] Y. Plotnik, M. C. Rechtsman, D. Song, M. Heinrich, J. M. Zeuner, S. Nolte, Y. Lumer, N. Malkova, J. Xu, A. Szameit, Z. Chen, and M. Segev, Nat. Mater. **13**, 57 (2013).
[42] B. A. Bernevig and T. L. Hughes, *Topological Insulators and Topological Superconductors* (Princeton University Press, Princeton, NJ, 2013).
[43] D. E. Chang, A. S. Sørensen, E. A. Demler, and M. D. Lukin, Nat. Phys. **3**, 807 (2007).
[44] B. Dayan, a. S. Parkins, T. Aoki, E. P. Ostby, K. J. Vahala, and H. J. Kimble, Science **319**, 1062 (2008).
[45] W. Chen, K. M. Beck, R. Bucker, M. Gullans, M. D. Lukin, H. Tanji-Suzuki, and V. Vuletic, Science **341**, 768 (2013).
[46] L. Neumeier, M. Leib, and M. J. Hartmann, Phys. Rev. Lett. **111**, 063601 (2013).
[47] I. Shomroni, S. Rosenblum, Y. Lovsky, O. Bechler, G. Guendelman, and B. Dayan, Science **345** (2014).
[48] B. Olmos, D. Yu, Y. Singh, F. Schreck, K. Bongs, and I. Lesanovsky, Phys. Rev. Lett. **110**, 143602 (2013).

[49] S. Stellmer, F. Schreck, and T. C. Killian, in *Annual Review of Cold Atoms and Molecules* (World Scientific Publishing Co., Singapore, 2014) pp. 1–80.
[50] T. Akatsuka, M. Takamoto, and H. Katori, Nat. Phys. **4**, 954 (2008).
[51] I. Bloch, Nat. Phys. **1**, 23 (2005).
[52] W. S. Bakr, A. Peng, M. E. Tai, R. Ma, J. Simon, J. I. Gillen, S. Folling, L. Pollet, and M. Greiner, Science **329**, 547 (2010).
[53] A. González-Tudela, C.-L. Hung, D. E. Chang, J. I. Cirac, and H. J. Kimble, Nat. Photonics **9**, 320 (2015).
[54] W. Yi, A. J. Daley, G. Pupillo, and P. Zoller, New J. Phys. **10**, 073015 (2008).
[55] S. Nascimbene, N. Goldman, N. R. Cooper, and J. Dalibard, Phys. Rev. Lett. **115**, 140401 (2015).
[56] F. Dolde, I. Jakobi, B. Naydenov, N. Zhao, S. Pezzagna, C. Trautmann, J. Meijer, P. Neumann, F. Jelezko, and J. Wrachtrup, Nat. Phys. **9**, 139 (2013).
[57] S. Kolkowitz, A. Safira, A. A. High, R. C. Devlin, S. Choi, Q. P. Unterreithmeier, D. Patterson, A. S. Zibrov, V. E. Manucharyan, H. Park, and M. D. Lukin, Science **347**, 1129 (2015).
[58] A. Sipahigil, R. E. Evans, D. D. Sukachev, M. J. Burek, J. Borregaard, M. K. Bhaskar, C. T. Nguyen, J. L. Pacheco, H. A. Atikian, C. Meuwly, R. M. Camacho, F. Jelezko, E. Bielejec, H. Park, M. Lončar, and M. D. Lukin, Science **354**, 847 (2016).
[59] T. Iwasaki, F. Ishibashi, Y. Miyamoto, Y. Doi, S. Kobayashi, T. Miyazaki, K. Tahara, K. D. Jahnke, L. J. Rogers, B. Naydenov, F. Jelezko, S. Yamasaki, S. Nagamachi, T. Inubushi, N. Mizuochi, and M. Hatano, Sci. Rep. **5**, 12882 (2015).
[60] Given the robustness of topological lattices, inhomogeneous broadening present in solid-state systems will not significantly change the results as long as the broadening is small compared to the topological energy gap.
[61] Q. H. Wang, K. Kalantar-Zadeh, A. Kis, J. N. Coleman, and M. S. Strano, Nat. Nanotechnol. **7**, 699 (2012).
[62] C. Robert, D. Lagarde, F. Cadiz, G. Wang, B. Lassagne, T. Amand, A. Balocchi, P. Renucci, S. Tongay, B. Urbaszek, and X. Marie, Phys. Rev. B **93**, 205423 (2016).
[63] H. Li, A. W. Contryman, X. Qian, S. M. Ardakani, Y. Gong, X. Wang, J. M. Weisse, C. H. Lee, J. Zhao, P. M. Ajayan, J. Li, H. C. Manoharan, and X. Zheng, Nat. Commun. **6**, 7381 (2015).
[64] C. Palacios-Berraquero, D. M. Kara, A. R. P. Montblanch, M. Barbone, P. Latawiec, D. Yoon, A. K. Ott, M. Loncar, A. C. Ferrari, and M. Atature, arXiv:1609.04244.
[65] Y. Lin, X. Ling, L. Yu, S. Huang, A. L. Hsu, Y.-H. Lee, J. Kong, M. S. Dresselhaus, and T. Palacios, Nano Lett. **14**, 5569 (2014).
[66] Y. Zhou, G. Scuri, D. S. Wild, A. A. High, A. Dibos, L. A. Jauregui, C. Shu, K. de Greve, K. Pistunova, A. Joe, T. Taniguchi, K. Watanabe, P. Kim, M. D. Lukin, and H. Park, arXiv:1701.05938.
[67] P. Back, M. Sidler, O. Cotlet, A. Srivastava, N. Takemura, M. Kroner, and A. Imamoglu, Phys. Rev. Lett. **118**, 237404 (2017).
[68] B. Hunt, J. D. Sanchez-Yamagishi, A. F. Young, M. Yankowitz, B. J. LeRoy, K. Watanabe, T. Taniguchi, P. Moon, M. Koshino, P. Jarillo-Herrero, and R. C. Ashoori, Science **340** (2013).
[69] C. Nayak, S. H. Simon, A. Stern, M. Freedman, and S. Das Sarma, Rev. Mod. Phys. **80**, 1083 (2008).
[70] Recently we became aware of a related study R. J. Bettles, J. Minář, I. Lesanovsky, C. S. Adams, and B. Olmos, arXiv:1703.03351.